liquids

MDPI

*Article*

# Modeling the Relationship Between the Transition Time and Energy Barrier in Films from Nanofluid Stepwise Thinning

**Jongju Lee * and Alex Nikolov**

Department of Chemical and Biological Engineering, Illinois Institute of Technology, Chicago, IL 60616, USA; nikolov@illinoistech.edu

* Correspondence: jlee210@hawk.iit.edu; Tel.: +1-312-567-5980

## Abstract

Liquid films formed from nanofluids exhibit a ubiquitous, multiple stepwise thinning phenomenon, where the film thins layer by layer. Under film confinement, the nanoparticles experience a significant reduction in their degrees of freedom, inducing entropy-driven structural transitions. The primary goal of this research is to model this oscillatory stepwise thinning behavior and predict the associated film thickness transition time. To achieve this, the oscillatory structural film free energy was quantified from the macroscopic contact angle of the film meniscus, providing a physically grounded measure of the energy barrier. As film thickness reduces, 2D in-layer structural ordering enhances, resulting in larger energy barriers and prolonged transition times. We present a power-law model relating the transition time to the corresponding free energy barrier. The fitted scaling exponent indicates a super-linear dependence, demonstrating that progressively thinner films resist thinning disproportionately due to confinement-induced cooperative ordering. This framework establishes a quantitative, predictive basis for understanding stepwise thinning (stratification) dynamics while offering practical insights for designing stable colloidal and interfacial assemblies.

**Keywords:** film from nanofluids; oscillatory stepwise thinning; film free energy barrier; transition time; power-law model; film-meniscus contact angle; film confinement; film stability

## 1. Introduction

Liquid films formed from monodisperse nano-colloidal suspensions exhibit a unique oscillatory, multiple stepwise thinning phenomenon that is of fundamental importance and has significant technological implications for the fabrication of nanostructured materials with tailored electrical and optical properties [1–4]. Such stepwise film thinning is a ubiquitous phenomenon that has been observed in foam, emulsion, and wetting films (see Figure 1).

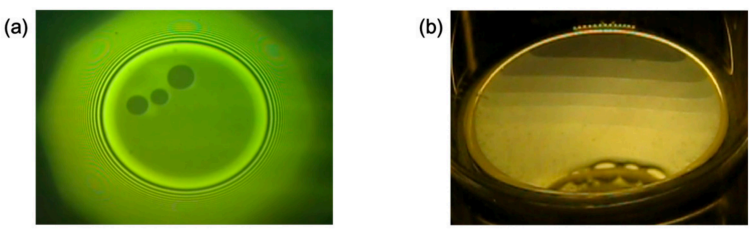



**Figure 1.** *Cont.*

Check for updates

Academic Editor: Antonio Fernandez-Barbero

Received: 25 July 2026
Revised: 27 August 2026
Accepted: 2 September 2026
Published: 7 September 2026

**Copyright:** © 2026 by the authors. Licensee MDPI, Basel, Switzerland. This article is an open access article distributed under the terms and conditions of the Creative Commons Attribution (CC BY) license.

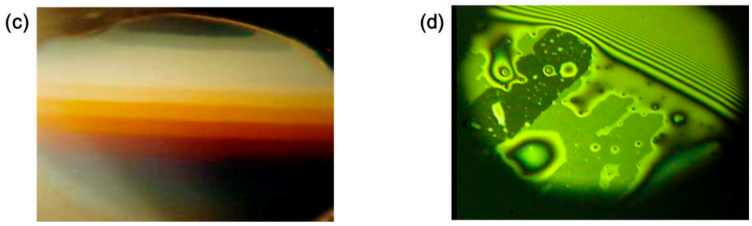



**Figure 1.** Examples of the stepwise thinning phenomenon in films: (**a**) horizontal micellar foam film [5] (micelle size = 11 nm, effective volume fraction = 0.3); (**b**) inclined micellar foam film [6] (micelle size = 9.8 nm, effective volume fraction = 0.4); (**c**) vertical latex foam film [7] (particle size = 156 nm, effective volume fraction = 0.44); and (**d**) horizontal silica particle film-meniscus on a solid surface [8] (particle size = 19 nm, effective volume fraction = 0.4). The variations in interference colors and grayscale contrast correspond to discrete differences in local film thickness resulting from stratification. Reproduced with permission from Refs. [5–8]: (**a**) Copyright 2014 Elsevier; (**b**) Copyright 2023 American Chemical Society; (**c**) Copyright 2023 Elsevier; (**d**) Copyright 2010 American Chemical Society.

However, the physical origin of the oscillatory, stepwise thinning behavior observed in films formed from monodisperse nano-colloidal suspensions cannot be fully explained within classical theoretical frameworks. The classical DLVO-based descriptions in this context have been discussed in detail in a recent comprehensive analysis by Nikolov et al. [7]. These studies demonstrate that confinement-induced ordering of nanoparticles or micelles gives rise to additional structural forces and associated free-energy barriers that are not predicted by classical DLVO theory. In a notable theoretical description, Kralchevsky et al. [9] modeled the metastable states of stratifying foam films within the classical DLVO framework, utilizing the Carnahan–Starling equation to estimate the structural contributions to the disjoining pressure. However, this approach fundamentally neglects the macroscopic effect of film size, overlooking the fact that thinning transitions are physically triggered by discrete in-layer particle organization within the confinement region. The theory falls short of capturing the true physical reality of the film thinning. Direct measurements of surface forces were enabled by the capillary force balance technique originally proposed by Scheludko-Exerowa [10,11]. Subsequent optical improvements introduced by Nikolov et al. [12,13] enabled high-resolution optical imaging of capillary surfaces, such as the film–meniscus region under high capillary pressure for small film sizes, using a long-working-distance, small-aperture M Plan 10×/0.14 Mitutoyo objective. These advances made it possible to resolve nanoscale thickness variations during film drainage and thinning. Using these techniques, it was demonstrated that foam, emulsion, and solid wetting films formed from colloidal suspensions undergo thickness reduction through discrete transitions under confinement, reflecting nanoparticle or micelle layering and in-layering structural transitions. Building on these advances, Nikolov and Wasan showed that self-organization of micelles and nanoparticles in confinement between film surfaces gives rise to oscillatory stepwise thinning governed by structural oscillatory forces [14,15]. Statistical–mechanical descriptions of these forces in confined colloidal films were subsequently developed, linking disjoining pressure concepts with particle-layer ordering [16]. Furthermore, theoretical simulations of hard-sphere fluids confined in wedge-shaped geometries, such as a film meniscus, have corroborated the structural layering phenomenon. Boda et al. [17] demonstrated that such confinement induces distinct density discontinuities and oscillatory pressure profiles due to the stepwise ordering of particle layers. These computational findings provide a fundamental thermodynamic basis for the in-layer structural ordering and oscillatory forces that govern the stepwise thinning process in macroscopic films. Structural ordering induced by the liquid-film confinement was also demonstrated in wedge-shaped colloidal systems, where discrete layering transitions were observed

between confining surfaces [18]. Subsequent optical investigations of wedge-like film–meniscus regions directly visualized two-dimensional nanoparticle ordering and showed that the resulting structural disjoining pressure modifies film spreading and stability [19]. Monte Carlo simulations later reproduced these confinement-induced structural regimes, confirming that electrostatic and excluded-volume interactions generate discrete layering and oscillatory normal forces under confinement [20]. Together, these findings indicate that geometrical confinement produces an oscillatory structural free-energy landscape in colloidal films.

As the micellar concentration exceeds the critical micelle concentration (CMC), micelles become confined between the two interfaces of the thinning film and undergo confinement-induced ordering. With the increasing confinement, initially disordered micellar layers evolve into layered and in-layered structures, leading to oscillatory, multiple stepwise thinning. The formation of these ordered structures gives rise to an oscillatory structural contribution to the film free-energy barrier, which alternates between repulsive and attractive regimes as the film thickness changes by approximately one micellar diameter [21,22]. Each thinning step corresponds to the expulsion of a single micellar layer and the crossing of a structural free-energy barrier, whose magnitude increases with confinement and micellar concentration, thereby opposing further thinning and stabilizing the film [23]. These confinement-induced structural free-energy barriers therefore provide a natural basis for interpreting the film thinning transitions in nano-colloidal films. However, despite extensive experimental evidence, a quantitative description linking the dynamics of individual thinning steps to the associated free-energy barriers remains incomplete.

The multiple stepwise thinning of foam, emulsion, and wetting films has motivated investigations using advanced optical techniques such as monochromatic reflected light interferometry, which provides direct insight into the mechanisms of liquid film stability. Using light interferometric techniques, Nikolov et al. [14] demonstrated that oscillatory, multiple stepwise thinning originates from nano- and micellar 2D layering within the film, giving rise to successive layer-by-layer thinning transitions. Direct evidence for oscillatory structural forces in supramolecular fluids was obtained by Kekicheff and Richetti using the surface force apparatus (SFA) [24]. Kralchevsky et al. [25] proposed the "vacancy-condensation mechanism" to describe discrete thinning transitions in micellar and colloidal films. Related interferometric studies also demonstrated that increased micellar polydispersity (for example, due to oil solubilization) reduces the free-energy barrier associated with stepwise thinning, thereby decreasing the film oscillatory structural forces and stability [5]. These light interferometric studies established the structural origin of stepwise thinning, motivating further investigations of stratification and drainage in specific surfactant systems.

Stepwise thinning of liquid films has been investigated over several decades using a range of experimental approaches. Langevin [26] reviewed and summarized extensive experimental studies on aqueous surfactant films, demonstrating that stratification and multistep thinning in sodium dodecyl sulfate (SDS)-based foam films arise from the combined effects of electrostatic interactions, micellar ordering, and surface rheology, with oscillatory structural forces governing film drainage and stability. Bergeron et al. [4] investigated stepwise thinning and stratified drainage in foam films stabilized by aqueous SDS, demonstrating that discrete thinning transitions occur via hole formation and sheeting under the combined action of the oscillatory disjoining pressure and capillary forces. Kristen and von Klitzing [27] showed that stepwise thinning in SDS-stabilized foam films is strongly influenced by electrostatic interactions and surfactant–polyelectrolyte complexation, with oscillatory structural forces governing film drainage above the polymer overlap concentration. In a related study, Zhang and Sharma [28] investigated stratification in foam

films formed from micellar SDS solutions and showed that stepwise thinning proceeds via the nucleation and growth of thinner circular domains governed by oscillatory structural disjoining pressure and coupled hydrodynamic effects. This domain nucleation and growth process can be comprehensively described by the vacancy-condensation model previously proposed by Kralchevsky et al. [25].

In this study, we establish a quantitative framework that relates the structural free-energy barrier to the transition time of individual thinning steps in nano-colloidal foam films. The analysis is based on reflected-light interferometric measurements of oscillatory thinning in micellar films, from which the characteristic lifetimes of successive layer-by-layer expulsion events are extracted. The corresponding free-energy barriers are independently determined and correlated with the transition times through a power-law relationship. This framework provides a physically constrained interpretation of stepwise thinning under confinement.

## 2. Materials and Methods

### *2.1. Materials*

Thin liquid films were formed from aqueous solutions of a nonionic surfactant, Enordet AE 1215-30 (Shell Chemical Company, Houston, TX, USA), a commercial ethoxylated alcohol with a paraffinic chain (C12–C15) and an average of 30 ethylene oxide units. Aqueous solutions were prepared using ultrapure water with a resistivity of 18.2 MΩ·cm (Milli-Q grade). The nonionic surfactant concentration was maintained at a fixed concentration of $5.2 \times 10^{-2}$ mol/L, which is above the critical micelle concentration (CMC) [15].

To validate the model across different surfactant charges, an ionic surfactant system was additionally evaluated using sodium dodecyl sulfate (SDS) at a concentration of 0.1 mol/L, which is well above the CMC [14].

### *2.2. Thin Liquid Film Formation*

Microscopic foam films were generated using a cylindrical ring capillary with a hydrophilic inner wall (radius = 1.5 mm). A biconcave-shaped drop was formed inside the ring, and liquid was withdrawn through a side orifice using a screw-driven piston pump to produce a horizontal film [14,15]. The film radius, and thus the capillary pressure acting on the film, was controlled by piston displacement. During the stepwise thinning process, the capillary pressure was fixed, resulting in an effectively constant film radius. Any possible radius variations associated with changes in disjoining pressure were below experimental resolution. Small pressure variations do not measurably affect the time intervals between successive transitions.

### *2.3. Monitoring of the Foam Film Stepwise Thinning*

The stepwise thinning of the foam films was monitored using reflected light interferometry (Figure 2). An optical bench equipped with a custom-built Mach–Zehnder interferometer with an M Plan 10×/0.14 objective (Mitutoyo Corporation, Kawasaki, Japan) was employed, in which monochromatic light (λ = 546 nm) was focused onto the film surface through the top of the thin ring with a hole from water-wet material (the cell). Light reflected from the film and meniscus surfaces interfered and produced fringes, which showed changes in the film thickness and meniscus profile during drainage.

The temporal evolution of the thinning film was continuously recorded using a CCD camera connected to a digital video acquisition system. For the interferometric analysis, the initial hydrodynamic drainage stage immediately following film formation was distinguished from the subsequent oscillatory stepwise thinning regime. The film thickness transition time, τ, is defined as the residence time of the film at a given thickness state prior

to a discrete, step-like transition to the next thinner state. This transition time depends strongly on the number of confined micellar layers ($n$), increasing exponentially as $n$ diminishes. For multilayer films ($n \geq 2$), the transition time corresponds to the period required for the initial dark spot(s) to nucleate and begin expanding, triggering the subsequent stepwise transition before the thinner domain fully covers the entire film area. In contrast, for a film containing a single micellar layer ($n = 1$), the intrinsic transition time is defined as the duration required for the dark spot to expand laterally across the entire film to reach the rim, thereby establishing a completely uniform thickness and achieving the macroscopic film–meniscus contact angle equilibrium.

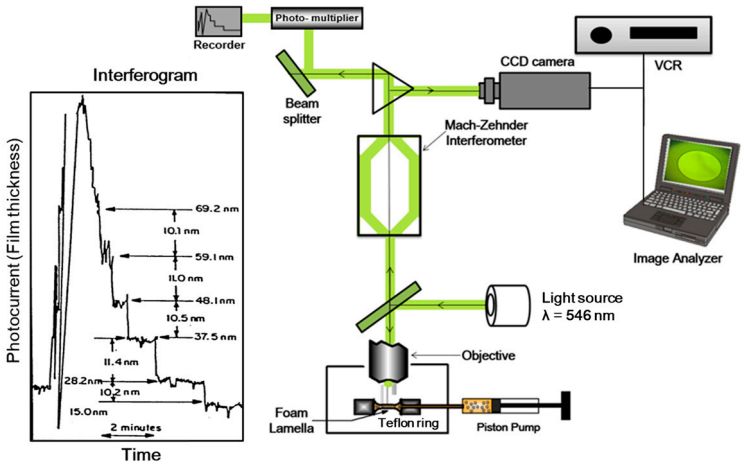



**Figure 2.** Schematic of the reflected light interferometric setup used to monitor the micellar foam film's multiple stepwise thinning [15]. The arrows indicate the optical path of the incident and reflected light.

Film thickness values were taken directly from the interferograms reported by Nikolov et al. [14,15], where thickness was determined using the Scheludko–Mysels interferometric formulation with the refractive index of the aqueous film.

### *2.4. Micellar Size Distribution Measurement*

Micellar solutions of the nonionic surfactant Enordet AE 1215-30 were characterized using dynamic light scattering (DLS). Measurements were performed using a ZETASIZER 3000HSA (Malvern Instruments, Worcestershire, UK) equipped with a helium–neon laser and integrated analysis software.

All measurements were conducted at a controlled temperature of 25 °C, with the scattering angle fixed at 90°. The hydrodynamic micellar size distributions were analyzed and are reported in terms of the z-average diameter and the polydispersity index (PDI).

## 3. Results and Discussions

### *3.1. Stepwise Thinning of Foam Films from Nanofluids Suspensions*

The film thinning experiments analyzed in this work were reported previously. The present study does not introduce a new parametric experimental campaign, but instead reanalyzes well-resolved published interferometric data to extract transition times, effective free energy barriers, and their quantitative correlation for the first time.

We first analyzed previously reported data from Nikolov et al. [15] concerning the drainage behavior of horizontal foam films formed from micellar solutions of the nonionic surfactant Enordet AE 1215-30. Specifically, we examined the time-resolved interferogram presented in Figure 9a in Nikolov et al. [15], corresponding to a surfactant concentration of

$5.2 \times 10^{-2}$ mol/L. From this interferogram, the transition times between the discrete film thicknesses were extracted.

The interferogram, recorded as the photocurrent signal directly proportional to the intensity of light reflected from the stratifying film, reveals a characteristic sequence of regular oscillatory, discrete thinning steps. Each plateau corresponds to the transition time of a film state, whereas the abrupt transitions denote the displacement of the individual micellar layer. The significance of this process arises from the combined effects of the micellar volume fraction, collective micellar interactions, and geometric confinement within the film. The film thickness represents a transient equilibrium configuration in which micelles form a 2D layered structure. The discreteness of these film thickness transitions demonstrates the robustness of micellar 2D self-layering under confinement [14].

Dynamic light scattering measurements yielded a z-average micelle diameter of $9.8 \pm 1$ nm with a low polydispersity index (PDI = 0.09) (see Figure A1, Appendix A). The average step height of the film thickness transition (~10 nm) is comparable to the measured micelle diameter, consistent with a layer-by-layer thinning mechanism in which each transition corresponds to the expulsion of a single micellar layer. This observation supports the interpretation that confinement-induced micellar ordering governs the stepwise thinning process.

Under confinement, spherical micelles self-organize into 2D random layers and a 2D structured in-layer, and drainage proceeds via sequential stepwise thinning [14]. Local instabilities, described by the "vacancy condensation mechanism", trigger the nucleation of dark spots—regions thinner by approximately one micellar layer relative to the surrounding film (Figure 3) [25]. The spot formation and expansion are governed by the balance between the micellar osmotic pressure ($P_{osm}$) and capillary pressure ($P_{cap}$). Nucleated dark spots initiate lateral expansion after reaching a critical radius of several micrometers. To rationalize this observation, the relative magnitudes of the opposing pressures must be considered. For a nonionic micellar film at a micelle concentration of $5.2 \times 10^{-2}$ mol/L, the osmotic pressure ($P_{osm}$) of dislocation is on the order of $1.27 \times 10^5$ Pa. The capillary pressure ($P_{cap}$) required to initiate the formation of a dark spot—corresponding to a film with one fewer micellar layer—corresponds to a critical radius of ~1.2 µm. This is consistent with interferometric observations showing that the dark spot's radius (film's local dislocation size) reaches 2–3 µm before expansion begins. Thus, the balance between local osmotic depletion and the opposing capillary pressure triggers the film's stepwise thinning.

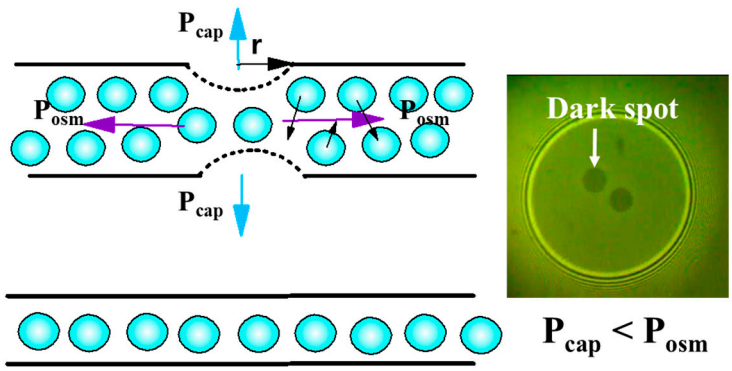



**Figure 3.** Local film instabilities are explained by the vacancy condensation mechanism. Dark spots nucleate and expand, and their growth is governed by the balance between the micellar osmotic pressure ($P_{osm}$) and capillary pressure ($P_{cap}$) within the dark spots. This pressure balance drives the stepwise thinning of the foam film. The blue and purple arrows indicate the directions of capillary pressure ($P_{cap}$) and micellar osmotic pressure ($P_{osm}$), respectively, while $r$ denotes the dark spot radius.

The dark spot expansion is driven by the diffusion of dislocations (vacancies) within the micellar lattice [29]. Vacancies generated at the film-meniscus migrate into the film and condense within the nucleated dark spot region, driving their lateral growth. Film confinement, particle layering, and the vacancy condensation mechanism explain the stepwise thinning of the film. Consequently, the stepwise thinning time of nano-colloidal foam films depends on the magnitude of the film free energy barrier, which increases as the film thickness decreases below three particle layers, where collective particle interactions become a dominant factor in the film free energy. Interferometric measurements revealed that the stepwise thinning transition time between successive thinning steps is governed by the magnitude of the film free energy barrier, confirming its role as the determinant of the film thickness transition time.

Nikolov et al. [15] reported that stepwise thinning in nonionic micellar films depends on the film area, temperature, effective volume fraction of the micelles, and electrolyte content. For example, at smaller areas or a higher micellar volume fraction, the film remains in stable multilayer states for longer periods. As the film thins, the film free energy barrier increases because the particles (micelles) become more ordered and form an in-layer structure [21]. The particle density near the film surfaces (walls) is high. Experimentally, it has been observed that films with smaller areas, thicknesses of two or one layers, and an effective particle volume fraction of 0.4 ceased thinning [15,22]. In films with smaller areas, the probability of dislocation (or vacancy) formation in the lattice is lower [30]. By monitoring the spot expansion rate, it is concluded that the flow rate of vacancies from the meniscus into the film drives the spot expansion and governs the film thickness transition time, rather than the film tension gradient or the osmotic pressure gradient. Consequently, reducing the film radius leads to a reduction in the spot expansion rate, thereby decreasing the film thickness transition time. Once the spot expansion is completed, the value of the film-meniscus contact angle directly depicts the state of the film free energy. Surface stresses, including Marangoni stresses, may in principle affect film drainage by altering interfacial mobility. In the present experiments, the surfactant concentration was maintained at approximately 860 times the CMC, leading to effectively immobilized film surfaces due to rapid micellar relaxation. Reflected light interferometry reveals a flat-shaped dimple with a thickness of less than 140 nm which appeared for less than a second (see Appendix B). Therefore, at a concentration 860 times the CMC, Marangoni-driven convection does not need to be considered as a factor; surface diffusion and interfacial elastic properties remain unchanged during a given thinning step. Consequently, the measured transition times reflect the intrinsic stepwise thinning dynamics at fixed interfacial boundary conditions rather than variations in surface stress.

### *3.2. Micellar/Nanoparticle Film Free Energy Isotherm*

The film–meniscus contact angle used in the evaluation of the structural free-energy barrier was determined from the film containing one particle layer. At this thickness, the film represents a well-defined state in which gravitational distortion of the meniscus curvature is minimized [31]. Because the film is thinner, hydrostatic pressure corrections to the meniscus profile are smaller, reducing uncertainty in the extracted contact angle. In addition, the interference fringes in the single-layer film are sharper and more symmetric than those observed in thicker films, enabling more accurate determination of the film thickness and curvature. For these reasons, the single-layer film provides the most reliable reference for constructing the oscillatory structural interaction energy isotherm, from which the free energy barriers of thicker films are obtained as relative quantities [29]. Furthermore, the effect of line tension (LT) on the macroscopic contact angle is mathematically and physically negligible for the macroscopic films (~100 μm radius) investigated in our study.

As theoretically discussed by Gibbs and Bakker, LT is primarily significant for micron-scale systems [32,33]. For macroscopic foam films, previous studies report that the LT values are on the order of $10^{-11}$ N, which makes its contribution to the contact angle several magnitudes smaller than our experimental measurement accuracy [34].

The relationship between the film free energy and the stepwise transition time reflects the correlation between the lifetime of a thickness state and the structural free-energy barrier associated with the stepwise thinning process. The film free energy isotherm constructed from the measured film–meniscus contact angle represents the interaction free energy per unit area arising from oscillatory structural forces within the confined film. Because the free energy is defined per unit film area, it arises from the interactions within the confined film and therefore does not depend explicitly on the size of the film. Instead, film size influences the overall stability and dynamics of the thinning process (the mechanism of stepwise thinning) through hydrodynamic drainage, capillary pressure, and the amplification of thickness fluctuations, which determine the film stability, lifetime of film states and the onset of thickness transitions [29,30]. In this sense, the power-law relation used in the present model provides a relationship between the transition time and the corresponding structural free-energy barrier. Therefore, the contact angle used in the energy calculation should correspond to a well-defined reference state of the film, which in the present analysis is taken as the film containing a single micellar layer.

The film free energy and corresponding barrier were calculated by applying the following equation [35]:

$$Acos\left(\frac{2\pi h}{d}\right)exp\left(-\frac{h}{d}\right) = 2\sigma_{a/l}(cos\theta_{mac} - 1) \quad (1)$$

where $A$ represents the film free energy oscillation amplitude, $\theta_{mac}$ denotes the interferometric measured macroscopic film-meniscus contact angle, $h$ is the film thickness, and $d$ is the effective diameter of the micelle/particle corresponding to the mean step size of the film thickness transitions. The surface tension, $\sigma_{a/l}$, was measured using the drop shape analysis method, where the apex radius of the curvature of the drop was obtained by fitting the drop profile with the Laplace equation [29]. Parameter $A$ was determined by selecting the film thickness and macroscopic film-meniscus contact angle that corresponded to a single micellar layer, representing the nature of the phenomenon. The film free energy per unit area ($W$) is expressed as follows [35]:

$$W = Acos\left(\frac{2\pi h}{d}\right)exp\left(-\frac{h}{d}\right) \quad (2)$$

The film free energy per unit area ($W$) was non-dimensionalized as $\frac{Wd^2}{kT}$. The film free energy barrier associated with each micellar layer was estimated by the film free energy isotherm, considering the positive branch as representative of the repulsive contribution (see Figure 4). Notably, as the number of micellar layers decreases, the repulsive component of the film free energy barrier increases exponentially, and the stepwise transition times become longer.

### 3.3. Modeling

The relationship between the film transition time ($\tau$) and the corresponding repulsive energy barrier ($\frac{\Delta Wd^2}{kT}$) was modeled using the power-law equation:

$$\frac{\Delta Wd^2}{kT} = a\left(\frac{\tau}{\tau_0}\right)^b \quad (3)$$

where $\frac{\Delta W d^2}{kT}$ represents the dimensionless repulsive film free energy barrier, $\tau$ is the film thickness transition time, $\tau_0$ is a characteristic time scale, defined from the initial thinning behavior, $a$ is a prefactor, representing the baseline of the energy barrier at $\tau = \tau_0$, and $b$ is the power-law exponent, determined via nonlinear least-squares regression. The exponent $b$ defines the sensitivity of the normalized structural barrier ($\frac{\Delta W d^2}{kT}$) to variations in the transition time $\tau$. When $b > 1$, the scaling is superlinear, indicating that even a modest increase in $\tau$ results in a disproportionately large rise in the barrier height. Physically, this scaling means that thinner, more confined films resist further thinning. Particle layering imposes cooperative constraints that cause the formation of a large energy barrier as the film becomes thinner, explaining the enhanced stability observed experimentally.

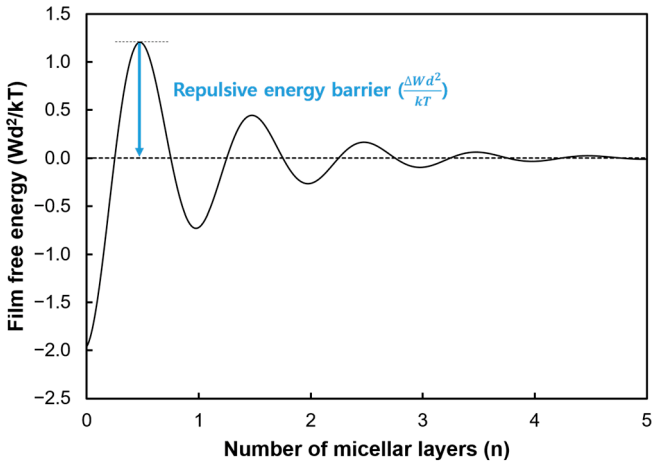



**Figure 4.** Dimensionless film free energy ($\frac{Wd^2}{kT}$) versus the number of micellar layers ($n$) for the $5.2 \times 10^{-2}$ mol/L Enordet AE 1215-30 micellar film ($\theta_{mac} = 1.47°$, $\sigma_{a/l} = 46.9$ mN/m, $d = 9.8$ nm) [15]. The repulsive energy barrier ($\frac{\Delta W d^2}{kT}$) corresponding to one micellar layer is indicated.

### *3.4. Model Prediction, Fitting, and Validation*

Building on the formulation presented in the previous section, we now evaluate the model predictions against the experimental data and examine the physical implications of the fitted parameters. The values of the film thickness transition time ($\tau$) and repulsive film free energy barrier ($\frac{\Delta W d^2}{kT}$) for the $5.2 \times 10^{-2}$ mol/L Enordet AE 1215-30 micellar film are presented in Table 1. These effective free energy barriers were extracted from a previously reported interferometric thinning trajectory; however, they were not reported or analyzed in the original experimental study.

**Table 1.** Film thickness transition time ($\tau$), repulsive film free energy barrier ($\frac{\Delta W d^2}{kT}$), and contact angle ($\theta_{mac}$) for the $5.2 \times 10^{-2}$ mol/L Enordet AE 1215-30 micellar film.

| Number of Micellar Layers, $n$ | Film Thickness Transition Time, $\tau$ (s) | Repulsive Film Free Energy Barrier, $\frac{\Delta W d^2}{kT}$ | Contact Angle, $\theta_{mac}$ (deg.) |
|---|---|---|---|
| 1 | 120 | 1.203 | $1.47 \pm 0.1$ |
| 2 | 66 | 0.443 | - |
| 3 | 42 | 0.163 | - |
| 4 | 32 | 0.060 | - |
| 5 | 12 | 0.022 | - |

In the case of the $5.2 \times 10^{-2}$ mol/L Enordet AE 1215-30 micellar film, the initial thinning behavior was referenced to the film containing five micellar layers. The film with five micellar layers was selected as the reference because, at this thickness, the particle

structure of the film is similar to that of the bulk phase and serves as the baseline. The characteristic transition time, $\tau_0$, was assigned a value of 12 s, corresponding to the thickness transition time of the film with five micellar layers, while the prefactor $a$ was set to 0.022, corresponding to the repulsive film free energy barrier of the same state. Substitution of $\tau_0$ and $a$ into Equation (3) yields the following equation:

$$\frac{\Delta W d^2}{kT} = 0.022\left(\frac{\tau}{12}\right)^b \quad (4)$$

The exponent $b$ in Equation (4) was determined using nonlinear least-squares regression implemented with the Solver optimization tool in Microsoft Excel (Microsoft 365, Microsoft Corporation, Redmond, WA, USA) by minimizing the sum of squared residuals between the Table 1 data and model predictions. This optimization yielded $b = 1.74$ with $R^2 = 0.995$. This result indicates a superlinear dependence of the film free energy barrier on the film thickness transition time. Equation (4) expresses the dimensionless repulsive film free energy barrier as a power law of the transition time for the $5.2 \times 10^{-2}$ mol/L Enordet AE 1215-30 micellar film. Accordingly, the barrier for each micellar layer can be evaluated directly from its measured transition time.

It is noted that the five discrete transition time data points represent a direct reflection of the physical phenomenon itself. The stepwise thinning process in these foam films proceeds through the layer-by-layer thinning of stratified micellar layers within the film. Each data point corresponds to a distinct, stable film thickness state characterized by a specific number of structured micellar layers. Therefore, replicating the measurement under identical thermodynamic and concentration conditions consistently yields the same five thickness states.

The model prediction based on Equation (4) was evaluated across a range of transition times and compared with the experimental data. As shown in Figure 5, the model captures the superlinear trend observed in the experimental values, with the repulsive film free energy barrier increasing rapidly as the film thins (i.e., as $\tau$ increases). The fitted exponent $b = 1.74$ reflects the sensitivity of the film free energy barrier to changes in the thinning dynamics. This superlinear behavior suggests that thinner films (with fewer micellar layers) experience disproportionately higher energy barriers, likely due to enhanced confinement and structural ordering effects. The agreement between the model and experimental data supports the validity of the power-law formulation.

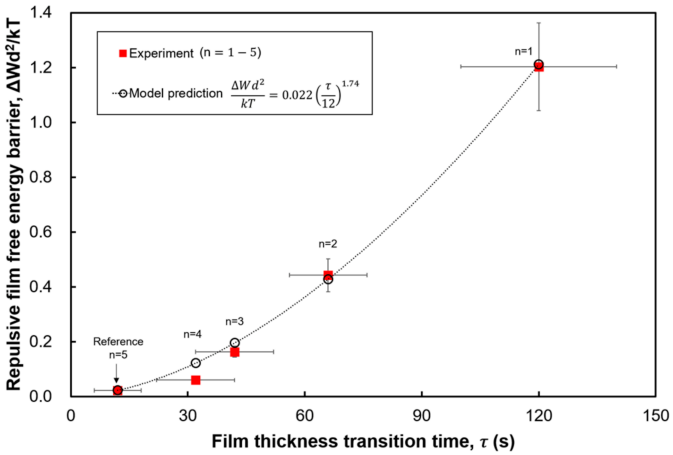



**Figure 5.** Repulsive film free energy barrier ($\frac{\Delta W d^2}{kT}$) versus film thickness transition time ($\tau$) for the $5.2 \times 10^{-2}$ mol/L Enordet AE 1215-30 micellar film. Squares denote experimental values with error bars for individual micellar layers ($n$ = 1–5); the film with the five-micellar-layer reference is indicated ($n = 5$; $\tau_0 = 12$ s; $a = 0.022$). Open circles represent the model prediction from Equation (4).

To validate the general applicability of the proposed power-law model, we extended our analysis to an ionic surfactant system using previously established interferometric data for a 0.1 mol/L SDS micellar foam film. The extracted transition times ($\tau$) from 0.1 mol/L SDS interferogram—shown in Figure A3 (originally Figure 3 in Ref. [14])—and corresponding dimensionless repulsive free energy barriers ($\frac{\Delta W d^2}{kT}$) for the SDS system are summarized in Table 2.

**Table 2.** Film thickness transition time ($\tau$), repulsive film free energy barrier ($\frac{\Delta W d^2}{kT}$), and contact angle ($\theta_{mac}$) for the 0.1 mol/L SDS film [14,25,36].

| Number of Micellar Layers, $n$ | Film Thickness Transition Time, $\tau$ (s) | Repulsive Film Free Energy Barrier, $\frac{\Delta W d^2}{kT}$ | Contact Angle, $\theta_{mac}$ (deg.) |
|---|---|---|---|
| 1 | 630 (220 *) | 1.110 | 0.906 |
| 2 | 112 | 0.405 | 0.790 |
| 3 | 56 | 0.150 | 0.685 |
| 4 | 24 | 0.055 | 0.665 |
| 5 | 12 | 0.021 | - |

(* Transition time by optical monitoring was 220 s based on direct visual observation, representing the actual duration required for the dark spot to fully expand to the film rim and establish a uniform thickness).

For the 0.1 mol/L SDS system, the film containing five micellar layers was similarly selected as the bulk reference state, defining the characteristic time scale $\tau = 12$ s and the baseline energy prefactor $a = 0.021$. Based on the vacancy condensation mechanism, dark spot nucleation and lateral expansion are highly dependent on the total influx of vacancies from the film meniscus, which is a function of the macroscopic film area (or volume). The 630 s transition time indicates that the finite size of the film restricted the vacancy concentration from reaching the critical threshold necessary for final dark spot formation. While reflected light interferometry accurately measures the vertical film thickness and the onset of a transition, it does not independently capture the lateral completion of the dark spot expansion. Visual observation is essential to confirm when the dark spot has fully reached the film's rim, thereby establishing a state of uniform thickness. Physically, a film must achieve this stable, uniform thickness across its entire area before the next stepwise transition can occur. During the experiment, it was visually confirmed that it takes approximately 220 s for the dark spot to fully expand to the rim. Therefore, the first-layer transition time was corrected to 220 s (see Appendix C).

To determine the revised scaling exponent ($b$), a nonlinear least-squares regression was performed using the adjusted dataset. By substituting the bulk reference parameters ($\tau_0 = 12$ s and $a = 0.021$) along with the corrected first-layer transition time (220 s) into Equation (3), the power-law exponent is $b = 1.36$. The resulting model equation for the 0.1 mol/L SDS micellar film is expressed as follows:

$$\frac{\Delta W d^2}{kT} = 0.021\left(\frac{\tau}{12}\right)^{1.36} \quad (5)$$

As illustrated in Figure 6, the power-law model successfully captures the superlinear relationship between the repulsive structural energy barrier and the film thickness transition time for the 0.1 mol/L SDS film. The optimized scaling exponent of $b = 1.36$ demonstrates that the film free energy barrier increases disproportionately as the film thins, driven by enhanced 2D in-layer ordering and structural constraints. Remarkably, this superlinear behavior closely aligns with the exponent obtained for the nonionic system (Enordet AE 1215-30) ($b = 1.74$), strongly implying that the scaling dynamics are fundamentally dictated by the nanoscale geometry of confinement.

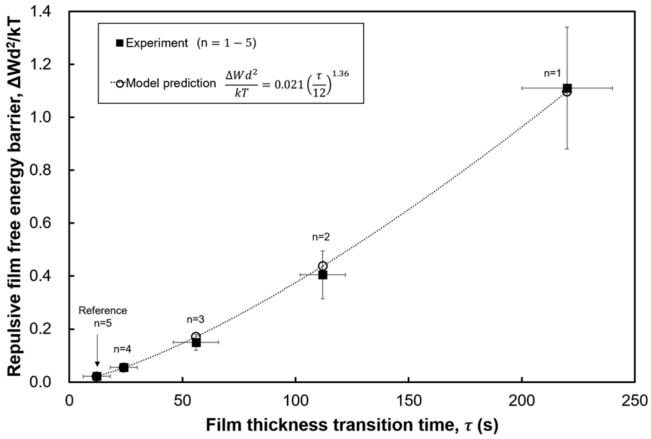



**Figure 6.** Repulsive film free energy barrier ($\frac{\Delta W d^2}{kT}$) versus film thickness transition time ($\tau$) for the 0.1 mol/L SDS micellar film. Squares denote experimental values with error bars for individual micellar layers ($n$ = 1–5); the film with the five-micellar-layer reference is indicated ($n = 5$; $\tau_0 = 12$ s; $a = 0.021$). Open circles represent the model prediction from Equation (5).

In summary, the multiple oscillatory stepwise thinning behavior of nano-colloidal films is governed by collective particle interactions and confinement-induced structuring. Under confinement, particles self-assemble into 2D layered and in-layered arrangements, giving rise to entropic structural transitions within the layers. Local fluctuations in the particle concentration within the film initiate stepwise thinning events (see Figure 3). The power-law relation thus provides a physically grounded description of the energetics of stepwise thinning, with the exponent $b$ serving as a quantitative measure of the cooperative dynamics underlying confinement-induced ordering. Although this geometric scaling physically applies to rigid, monodisperse colloidal particles under confinement, the present model cannot be directly applied to films stabilized with Janus particles, where distinct surface domains and directional interfacial orientations introduce complex boundary phenomena. Furthermore, for soft, deformable colloids (such as dendrimers and microgels), internal elasticity, steric compressibility, and shape fluctuations may alter the quantitative scaling exponent. Therefore, extending the present framework to such complex or deformable systems remains a subject for dedicated experimental verification under comparable confinement conditions.

## 4. Conclusions

In this work, we have shown that the oscillatory multiple stepwise thinning of liquid films formed from micellar dispersions originates from oscillatory variations in the film free energy arising from confinement-induced particle layering. Under confinement, micelles or nanoparticles self-organize into layered structures within the film, leading to a sequence of metastable thickness states separated by discrete thinning transitions.

The oscillatory film free energy associated with these transitions was quantified using the macroscopic contact angle of the film meniscus, providing a physically grounded measure of the free energy barrier corresponding to each thinning step. On this basis, a power-law relationship was established between the film thickness transition time and the associated free energy barrier, enabling a quantitative kinetic description of stepwise thinning.

The fitted scaling exponent ($b$) reveals that confinement-induced collective particle interactions drive entropy-driven structural transitions within the film, indicating that progressively thinner micellar films exhibit a resistance to thinning as structural constraints become increasingly pronounced. Overall, the present framework provides a quantitative and physically interpretable description of the stability and thinning dynamics of stratifying films formed from colloidal dispersions, elucidating how confinement-induced structural

forces and cooperative particle ordering govern the lifetime of colloidal and interfacial systems. While the underlying geometric scaling applies to rigid colloidal particles under confinement, extending the proposed quantitative framework to films stabilized with Janus particles (amphiphilic) or deformable soft-particle systems (such as dendrimers and microgels) remains a subject for future experimental validation.

**Author Contributions:** Conceptualization and writing—original draft preparation, A.N.; writing—original draft preparation and writing—review and editing, J.L. All authors have read and agreed to the published version of the manuscript.

**Funding:** This research received no external funding.

**Data Availability Statement:** The data presented in this study are available on request from the corresponding author.

**Conflicts of Interest:** The authors declare no conflicts of interest.

## Abbreviations

The following abbreviations are used in this manuscript:

| | |
|---|---|
| DLVO | Derjaguin–Landau–Verwey–Overbeek |
| CMC | Critical Micelle Concentration |
| DLS | Dynamic Light Scattering |
| PDI | Polydispersity Index |
| SDS | Sodium Dodecyl Sulfate |
| SFA | Surface Force Apparatus |
| LT | Line Tension |

## Appendix A. Dynamic Light Scattering (DLS) Analysis of Micellar Solutions

Micellar solutions of the nonionic surfactant Enordet AE 1215-30 were characterized by dynamic light scattering (DLS). Measurements were performed using a Zetasizer 3000HSA (Malvern Instruments Ltd., Worcestershire, UK) equipped with a He–Ne laser and integrated data analysis software. All measurements were conducted at 25 °C with a fixed scattering angle of 90°. The hydrodynamic size distributions were analyzed in terms of the z-average diameter and the polydispersity index (PDI). The results are shown in Figure A1.

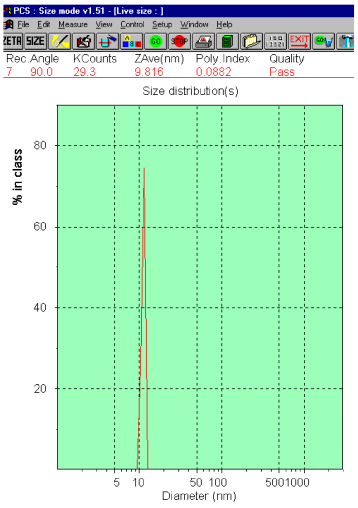



**Figure A1.** Hydrodynamic micelle size distribution of Enordet AE 1215-30 measured by dynamic light scattering at 25 °C and a scattering angle of 90°. The z-average diameter is 9.8 nm with a polydispersity index of 0.09.

## Appendix B. Evaluation of the Role of Marangoni Stresses via Dimple Effect Monitoring

The dynamic influence of the Marangoni effect on thin liquid film drainage is typically expected at surfactant concentrations below or around the CMC. To evaluate the interfacial mobility, we monitored the dimple formation and evolution using monochromatic reflected light interferometry for the $5.2 \times 10^{-2}$ mol/L Enordet AE 1215-30 film. As demonstrated by the interferogram (see Figure A2), the confined liquid film exhibits a highly stable, symmetric, and flat-shaped dimple configuration immediately following the initial hydrodynamic transition, displaying only one or two distinct geometric patterns. In the case of the $5.2 \times 10^{-2}$ mol/L Enordet AE 1215-30 solution, the concentration is approximately 860 times above the CMC, ensuring a Gibbs elasticity orders of magnitude above the immobilization baseline. Rapid micellar relaxation instantaneously dampens any flow-induced interfacial gradients. Consequently, the flat shape of the dimple confirms that Marangoni stresses do not serve as a contributing factor to the stepwise film thinning.

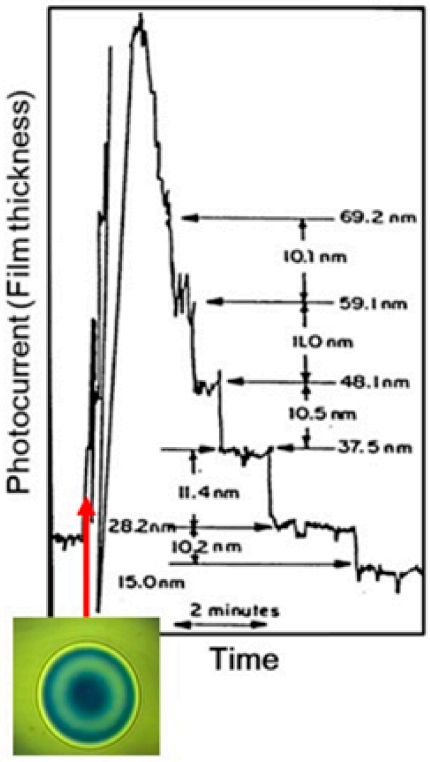



**Figure A2.** Interferometric observation of the dimple configuration during the initial film formation in the case of the $5.2 \times 10^{-2}$ mol/L Enordet AE 1215-30 film. The red arrow indicates the appearance of the dimple stage during initial hydrodynamic drainage, and the inset photograph represents the dimple formation in the film.

## Appendix C. Photocurrent Versus Time Interferograms of a 0.1 mol/L SDS Film

The stepwise thinning of the 0.1 mol/L SDS micellar foam film was evaluated by coordinating monochromatic reflected light interferometry. As illustrated in Figure A3, the total film thickness transition time for the film with 1 micellar layer ($n = 1$) approximately 630 s. Direct visual monitoring of the film, however, demonstrates that this total duration encompasses two fundamentally distinct physical regimes. The first phase takes approximately 220 s, during which a nucleated dark spot undergoes active lateral expansion under the driving force of the local micellar chemical potential gradient until it reaches the film's

rim. At the end of this 220 s period, the film achieves a completely uniform single-layer thickness over its entire area. Once this structural transition is completed laterally, the film enters the second phase, remaining stable as a uniform equilibrium film for an additional ~410 s. This prolonged stability interval is governed by finite-size constraints, where the restricted film area limits the localized vacancy accumulation necessary to fluctuate and trigger the subsequent dark spot nucleation for the final transition. This correction applies only to the film with 1 micellar layer ($n = 1$). For the film with multi-micellar layers ($n = 2$–5), the interferometrically measured plateau duration directly corresponds to the intrinsic thinning transition and therefore no correction was required. The $n = 1$ state is unique because the measured plateau contains an additional equilibrium-stability interval following completion of the lateral dark-spot expansion.

Therefore, by utilizing visual observation to decouple the actual lateral transition duration (220 s) from the subsequent stability period, the intrinsic transition time can be isolated to calibrate the superlinear scaling parameters in the power-law model accurately. In essence, the 220 s expansion time was employed because it exclusively captures the true structural resistance of micellar layer expulsion. Using the full 630 s interval would mathematically distort the model by introducing finite-size stability delays that are independent of the intrinsic thinning process.

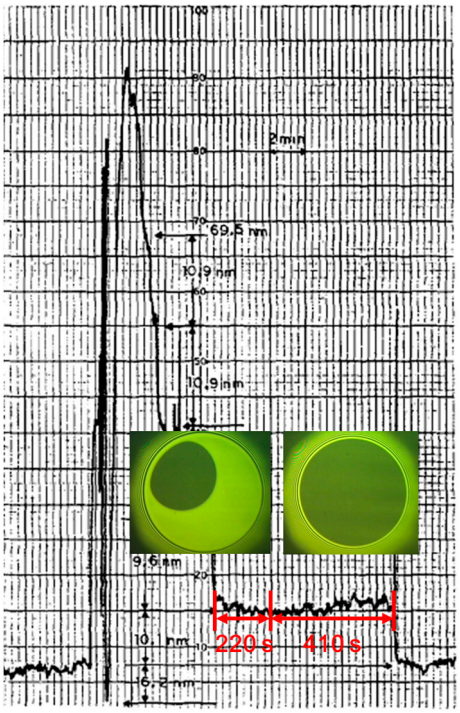



**Figure A3.** Photocurrent versus time interferogram of the 0.1 mol/L SDS film. Inset micrographs illustrate the visual decoupling of the total 630 s plateau into the intrinsic 220 s dark spot lateral expansion phase and the remaining 410 s uniform, equilibrium phase. (Reproduced from Nikolov and Wasan [14] with permission from Elsevier).

## References

1. Marinova, K.; Gurkov, T.; Dimitrova, T.; Alargova, R.; Smith, D. Role of oscillatory structural forces for interactions in thin emulsion films containing micelles. *Langmuir* **1998**, *14*, 2011–2019. [CrossRef]
2. Kralchevsky, P.A.; Danov, K.D.; Anachkov, S.E. Depletion forces in thin liquid films due to nonionic and ionic surfactant micelles. *Curr. Opin. Colloid Interface Sci.* **2015**, *20*, 11–18. [CrossRef]

3. Anachkov, S.E.; Danov, K.D.; Basheva, E.S.; Kralchevsky, P.A.; Ananthapadmanabhan, K.P. Determination of the aggregation number and charge of ionic surfactant micelles from the stepwise thinning of foam films. *Adv. Colloid Interface Sci.* **2012**, *183*, 55–67. [CrossRef]
4. Bergeron, V.; Jimenez-Laguna, A.; Radke, C. Hole formation and sheeting in the drainage of thin liquid films. *Langmuir* **1992**, *8*, 3027–3032. [CrossRef]
5. Lee, J.; Nikolov, A.; Wasan, D. Surfactant micelles containing solubilized oil decrease foam film thickness stability. *J. Colloid Interface Sci.* **2014**, *415*, 18–25. [CrossRef]
6. Nikolov, A.D.; Lee, J.; Wasan, D. Rheology of a Foam Film Formed from a Nanofluid: Role of the Structural Transitions. In *Proceedings of the One Hundred Years of Colloid Symposia: Looking Back and Looking Forward*; American Chemical Society: Washington, DC, USA, 2023; pp. 65–73.
7. Nikolov, A.; Lee, J.; Wasan, D. DLVO surface forces in liquid films and statistical mechanics of colloidal oscillatory structural forces in dispersion stability. *Adv. Colloid Interface Sci.* **2023**, *313*, 102847. [CrossRef]
8. Nikolov, A.; Kondiparty, K.; Wasan, D. Nanoparticle self-structuring in a nanofluid film spreading on a solid surface. *Langmuir* **2010**, *26*, 7665–7670. [CrossRef]
9. Kralchevsky, P.A.; Danov, K.D.; Ivanov, I.B. Thin Liquid Film Physics. In *Foams and Foam Films*; Exerowa, D., Kruglyakov, P., Eds.; Marcel Dekker: New York, NY, USA, 1995; pp. 1–114.
10. Scheludko, A.; Exerowa, D. Instrument for interferometric measuring of the thickness of microscopic foam layers. *Commun. Inst. Chem. Bulg. Acad. Sci.* **1959**, *7*, 123–131.
11. Sheludko, A. Thin liquid films. *Adv. Colloid Interface Sci.* **1967**, *1*, 391–464. [CrossRef]
12. Nikolov, A.D.; Dimitrov, A.S.; Kralchevsky, P.A. Accuracy of the Differential-interferometric Measurements of Curvature. *Opt. Acta Int. J. Opt.* **1986**, *33*, 1359–1368. [CrossRef]
13. Nikolov, A.D.; Wasan, D.T. Fluid-fluid interfaces: Optical imaging of capillary systems. In *The Handbook of Surface Imaging and Visualization*; CRC Press: Boca Raton, FL, USA, 2022; pp. 209–214.
14. Nikolov, A.; Wasan, D. Ordered micelle structuring in thin films formed from anionic surfactant solutions: I. Experimental. *J. Colloid Interface Sci.* **1989**, *133*, 1–12. [CrossRef]
15. Nikolov, A.; Wasan, D.; Denkov, N.; Kralchevsky, P.; Ivanov, I. Drainage of foam films in the presence of nonionic micelles. In *Proceedings of the Surfactants and Macromolecules: Self-Assembly at Interfaces and in Bulk*; Steinkopff Verlag: Darmstadt/Heidelberg, Germany, 1990; pp. 87–98.
16. Trokhymchuk, A.; Henderson, D.; Nikolov, A.; Wasan, D.T. A simple calculation of structural and depletion forces for fluids/suspensions confined in a film. *Langmuir* **2001**, *17*, 4940–4947. [CrossRef]
17. Boda, D.; Chan, K.-Y.; Henderson, D.; Wasan, D.T.; Nikolov, A.D. Structure and pressure of a hard sphere fluid in a wedge-shaped cell or meniscus. *Langmuir* **1999**, *15*, 4311–4313. [CrossRef]
18. Pieranski, P. Colloidal crystals. *Contemp. Phys.* **1983**, *24*, 25–73. [CrossRef]
19. Wasan, D.T.; Nikolov, A.D. Spreading of nanofluids on solids. *Nature* **2003**, *423*, 156–159. [CrossRef]
20. Trokhymchuk, A.; Henderson, D.; Nikolov, A.; Wasan, D.T. Computer simulation of macroion layering in a wedge film. *Langmuir* **2005**, *21*, 10240–10250. [CrossRef]
21. Chu, X.; Nikolov, A.; Wasan, D. Monte Carlo simulation of inlayer structure formation in thin liquid films. *Langmuir* **1994**, *10*, 4403–4408. [CrossRef]
22. Wasan, D.; Nikolov, A.; Henderson, D. New vistas in dispersion science and engineering. *Am. Inst. Chem. Eng. AIChE J.* **2003**, *49*, 550. [CrossRef]
23. Nikolov, A.D.; Wasan, D.T. Micellar films: Thinning and structure. In *Encyclopedia of Surface and Colloid Science*, 2nd ed.; Taylor & Francis: Abingdon, UK, 2008; pp. 1–17.
24. Kekicheff, P.; Richetti, P. Direct measurement of interactions in supermolecular fluids and liquid crystals. *Pure Appl. Chem.* **1992**, *64*, 1603–1609. [CrossRef]
25. Kralchevsky, P.; Nikolov, A.; Wasan, D.; Ivanov, I. Formation and expansion of dark spots in stratifying foam films. *Langmuir* **1990**, *6*, 1180–1189. [CrossRef]
26. Langevin, D. On the rupture of thin films made from aqueous surfactant solutions. *Adv. Colloid Interface Sci.* **2020**, *275*, 102075. [CrossRef]
27. Kristen, N.; von Klitzing, R. Effect of polyelectrolyte/surfactant combinations on the stability of foam films. *Soft Matter* **2010**, *6*, 849–861. [CrossRef]
28. Zhang, Y.; Sharma, V. Domain expansion dynamics in stratifying foam films: Experiments. *Soft Matter* **2015**, *11*, 4408–4417. [CrossRef]
29. Lee, J.; Nikolov, A.; Wasan, D. Stratification of a foam film formed from a nonionic micellar solution: Experiments and modeling. *Langmuir* **2016**, *32*, 4837–4847. [CrossRef]

30. Nikolov, A.D.; Wasan, D.T. The foam film's stepwise thinning phenomenon and role of oscillatory forces. *Adv. Colloid Interface Sci.* **2022**, *303*, 102636. [CrossRef]
31. Nikolov, A.; Wu, P.; Wasan, D. Novel approach for calculating the equilibrium foam nanofilm-meniscus contact angle and the film free energy. *J. Colloid Interface Sci.* **2019**, *557*, 591–597. [CrossRef]
32. Bakker, G. *Kapillarität und Oberflächenspannung*; Akademische Verlagsgesellschaft: Leipzig, Germany, 1928; Volume 6.
33. Gibbs, J.W. *Scientific Papers: Thermodynamics*; Dover Publications: Garden City, NY, USA, 1961; Volume 1.
34. Nikolov, A.; Kralchevsky, P.; Ivanov, I. A New Method for Measuring Film and Line Tensions. In *Surfactants in Solution: Volume 6*; Springer: Berlin/Heidelberg, Germany, 1986; pp. 1537–1547.
35. De Feijter, J.; Rijnbout, J.; Vrij, A. Contact angles in thin liquid films. I. Thermodynamic description. *J. Colloid Interface Sci.* **1978**, *64*, 258–268. [CrossRef]
36. Lee, J.; Nikolov, A.; Wasan, D. Stepwise thinning dynamics of a foam film formed from an anionic micellar solution. *J. Colloid Interface Sci.* **2017**, *487*, 217–222. [CrossRef]

**Disclaimer/Publisher's Note:** The statements, opinions and data contained in all publications are solely those of the individual author(s) and contributor(s) and not of MDPI and/or the editor(s). MDPI and/or the editor(s) disclaim responsibility for any injury to people or property resulting from any ideas, methods, instructions or products referred to in the content.